

# Off line Parallax Correction for Neutral Particle Gas Detectors.

P. Van Esch

August 28, 2018

## Abstract

In a neutral particle gas detector, the parallax error resulting from the perpendicular projection on the detection plane or wire of the radial particle trajectories emanating from a point like source (such as a scattering sample) can significantly spoil the apparent angular resolution of the detector. However, as we will show, the information is not lost. We propose an off line data treatment to restore as much as possible the original scattering information in the case of a one-dimensional parallax effect. The reversibility of parallax follows from the algebraic structure of this effect, which is different from the resolution loss which is essentially irreversible. The interplay between finite resolution and parallax complicates the issue, but this can be resolved.

## 1 Introduction

The parallax effect occurs when a point like source emits radiation along spherically radial lines, which is then detected by a detector with finite thickness and whose detection mechanism projects this radial trajectory onto a plane or onto a line (wire). This typically occurs in gas detectors of neutral particles, as shown in figure 1: the neutral particle follows its radial trajectory throughout the 'conversion volume' where it suffers an exponentially distributed probability to give rise to a cloud of electrical charge (to convert). This charge then follows electrical drift field lines until it reaches a position sensitive detection element (such as a wire or a micro strip detection element). Usually, for construction reasons, these drift field lines are perpendicular to the detection surface or line. So the conversion point (which is randomly distributed along the radial line) will be projected perpendicularly onto the detection element. A narrow particle beam will thus give rise to a smeared-out spot. This smearing-out effect is called the parallax effect. One tends to confuse it often with resolution loss, but we will show in this paper that the algebraic structure of the operator corresponding to 'parallax effect' is reversible, while 'resolution loss' is essentially irreversible. We will also work out the reverse operation in theory and in a simulated example.

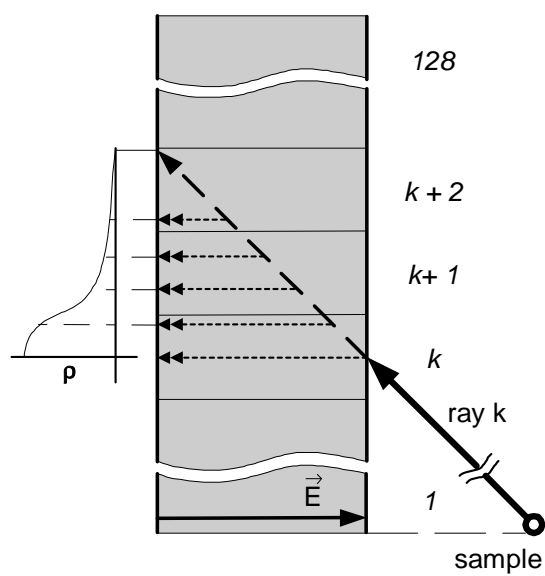


Figure 1: The principle of the parallax effect: a ray from the sample, hitting bin  $k$ , also gives rise to a conversion probability in the next few bins.

We haven't found much literature concerning this issue ; the idea of inverting the parallax operator was suggested in [1] in a JINR internal report; but it was specified that the method gave problems when the detector had finite resolution. Most people try to correct the detector hardware to avoid parallax, such as [2] and [3] by adapting the entire detection volume, or [4], taken over by [5], by trying to correct for the electric field projection. An overview of hardware correction techniques is given in the review [6].

In this paper we will focus on the algebraic structure of the parallax effect on the image, and how to inverse it, even in the case of finite resolution. We will work out explicitly the case of two geometries: a rectangular volume with projection perpendicular on a plane, and a cylindrical volume with projection onto a wire. In both cases, we only consider the parallax in one dimension. We will subdivide this relevant dimension in 128 position bins, so an image consists of 128 intensities. We will have the 'true image'  $I_{\text{true}}(n)$  which represents the intensity of entering neutral particles in each bin (at the entrance window level). We have the conversion image  $I_{\text{para}}(n)$ , which is the perpendicular projection of the conversion points, due to the parallax effect. Finally, we have the raw image,  $I_{\text{raw}}(n)$ , which is the conversion image with the finite resolution of the detection element.

## 2 Algebraic structure of the parallax and resolution operators.

### 2.1 Resolution and convolution.

In the continuum limit (an infinite number of infinitesimal bins), finite resolution comes down to the convolution of the original image with the point response of the detector describing its resolution. This point response is usually very well modelled by a gaussian distribution but this can be any function with a single extremum. This operation can be seen as the application of a linear operator on the image function:

$$i_{\text{instrument}}(x) = \int dy g(x-y) i_{\text{true}}(y) \quad (1)$$

As it is well known, the translation invariance of this operator results in eigenfunctions which are complex exponentials; in other words, the operator is made diagonal by a Fourier transform. The discrete version of this operation in the case of an infinite train of samples, or a finite number of cyclic samples, is at the heart of digital signal processing, as explained in [7]. We work however with a finite number of bins in our detector, which are not to be considered cyclic. As such, Fourier representation (or the Z-transform) cannot really be applied so we have to consider the operator on the image as a general linear operator:

$$i_{\text{instrument}}(n) = \sum_{k=1}^N g_{n,k} i_{\text{true}}(k) \quad (2)$$

The square matrix  $g_{n,k}$  then consists of columns which are given by:

$$g_{n,k} = G(n - k) \quad (3)$$

and  $G(l)$  is the sampled point response of the detector. There is still of course a spectral representation: the eigenvalues of the matrix  $g_{n,k}$ . This spectral representation is what comes closest to the Fourier representation. As an example, let us consider 128 bins with  $G(k) = e^{-\frac{k^2}{4}}$ . This is a gaussian point response that has a full width half maximum of 3.3 bins. The matrix  $g_{n,k}$  is a symmetrical matrix if the point resolution function is symmetrical. Constructing the corresponding matrix, and solving for the eigenvalues, we find the distribution given in figure 2. If this were a true Fourier representation, we would talk about a low pass filter. The ratio of the highest to the lowest eigenvalue is about  $10^4$ , which indicates that this is a highly irreversible operator in practice. This is somehow normal: a low pass filter has irreversibly cut away the high frequency components. In our case, it has irreversibly cut away the projection onto the eigenvector images corresponding to the small eigenvalues.

## 2.2 The parallax operator.

The parallax effect, even in the continuum limit, can not be written as a convolution of the image with a kind of 'parallax kernel function', because the parallax effect is strongly position dependent. But of course it is still a linear operator, so we can write its effect always as:

$$i_{\text{instrument}}(n) = \sum_{k=1}^N p_{n,k} i_{\text{true}}(k) \quad (4)$$

Because even in the continuum limit this operator is not a convolution, there is no remote resemblance to a Fourier representation. In order to look closer at the structure of the matrix  $p$ , we will have to think about the physical process that is at the origin of the parallax effect. We will assume, as shown in figure 1, that bin 1 of our 128 bins is perfectly perpendicular to the sample ray, so that no parallax occurs, and that the effect becomes stronger because the projection direction deviates more and more from the radial direction as the bin number increases. The general structure of the matrix  $p_{n,k}$  is a sparse lower-triangular matrix, each column containing the 'parallax tail' of a thin ray leaking in the next few bins. The diagonal elements are nothing else but the fraction of particles in the ray hitting bin  $k$  that will also convert in bin  $k$ . This is determined by the geometry of the conversion volume, its binning and the absorption law for the neutral particles. The diagonal elements, which are also the eigenvalues for a triangular matrix, will not vary wildly. In figure 2, the eigenvalues of such an operator are displayed. *It is from this observation that the reversibility of the parallax effect results.* Indeed, the eigenvalues all having comparable values, the condition number of the matrix will not be very high, and the inverse matrix will be numerically very well defined. A remark is maybe

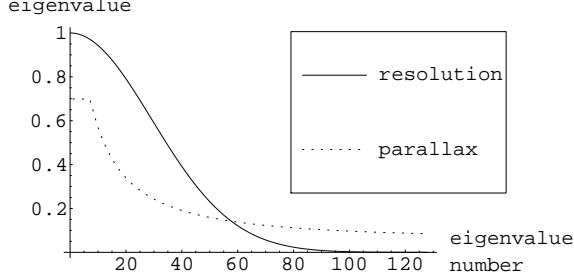


Figure 2: The eigenvalues of the operators  $G$  and  $P$  corresponding respectively to a gaussian point response  $G(k) \sim e^{-\frac{k^2}{4}}$  and the parallax in the case of a rectangular detection volume, over 128 bins, in descending order.

due: although very regular, the matrix may be badly scaled, so some care is to be taken in choosing the numerical inversion technique. If the detector had perfect resolution (meaning that  $G(m) \approx \delta_{m,0}$ ), then this would be the end of the story.

### 2.3 Combination of resolution and parallax.

In the previous two subsections we analyzed the algebraic structure of the linear operator  $G$  that implements finite resolution of the detector and the operator  $P$  that implements the parallax effect. But in a real detector, both effects occur. From the different structure of the eigenvectors, it is clear that  $G$  and  $P$  do not commute. We will assume here that the finite resolution is an effect that occurs after the parallax effect has had its effect, as usually is the case in neutral (and even sometimes in charged) particle detectors: indeed, the trajectory of the primary particle, before conversion into a charge cloud, is usually only affected by the geometry (parallax). Most other (resolution) effects (finite spread of charge, diffusion, electronic noise etc...) occur afterwards. We hence have:

$$I_{\text{para}} = P I_{\text{true}} \quad (5)$$

and:

$$I_{\text{raw}} = G I_{\text{para}} = G P I_{\text{true}} \quad (6)$$

Because  $G$  is nearly singular, we can't inverse the last equation, so our hope to recover  $I_{\text{true}}$  from  $I_{\text{raw}}$  vanishes. But that is normal, we know that we will suffer from the resolution loss, and the parallax effect will certainly not improve on this. However, we would like to recover  $I_{\text{nopara}} = G I_{\text{true}}$ , that is, the image that has the resolution of the detector but doesn't suffer from parallax anymore.

Formally, can write:

$$I_{\text{nopara}} = G(GP)^{-1}I_{\text{raw}} \quad (7)$$

but again, because of the singular character of  $G$  this is not workable as such. It would have been if  $P$  and  $G$  commuted, but they don't. However, we can now apply a truncated singular value decomposition on  $GP$  as explained in [8]:

$$GP \approx U^T \Sigma V \quad (8)$$

where we limit the diagonal matrix  $\Sigma$  to those eigenvalues of  $GP$  that are significant (it is our choice to specify what we call significant: usually, given the numerical precision of the data on which we will work, something of the order of 1% or 10% will do). What has been done here is replacing the numerically near-singular matrix  $GP$  by a numerically regular matrix  $\Sigma$  of lower rank (the number of accepted eigenvalues), and two orthogonal projection operators  $U$  and  $V$ . As such, we can work out equation 7:

$$I_{\text{nopara}} \approx I_{\text{sol}} = GV^T \Sigma^{-1} U I_{\text{raw}} \quad (9)$$

The solution proposed in equation 9 is numerically stable, but one should keep in mind that it is an approximation. Indeed, eigenvectors of  $GP$  with a small eigenvalue (which are thrown away in the truncated singular value decomposition) could have large parts of eigenvectors of  $G$  with large eigenvalues, hence contributing to the solution. However, there is no way to calculate in a numerically stable way these contributions, so there's more chance that they introduce spurious terms than improve upon the solution. By using a truncated singular value decomposition, we've thrown away all these potentially dangerous contributions, but at the same time also their true contribution.

### 3 Test cases.

#### 3.1 Case of a rectangular drift volume.

To calculate the parallax operator in the case of a rectangular drift volume, we consider a ray  $k$  that hits the entrance window in the middle of the  $k^{\text{th}}$  bin and calculate the distances  $s_j$  travelled on this ray from that point on to each of the bin boundaries. The entry in the matrix for a particular bin is then simply given by:

$$p_{k+j,k} = e^{-\mu s_j} - e^{-\mu s_{j+1}} \quad (10)$$

This corresponds to the probability of conversion in bin  $k+j$ . We consider the example of a rectangular drift volume with depth 3cm, a height of 40cm divided into 128 position bins and a sample distance of 40cm. The absorption coefficient is put to 0.4 absorption lengths per cm. The resolution of the detector (FWHM) is 3.7 bins. If we just generate a test picture, and see how the picture is affected if (1) we only had the finite resolution of the detector, or if (2) we had parallax and the finite resolution of the detector, we obtain the images displayed in

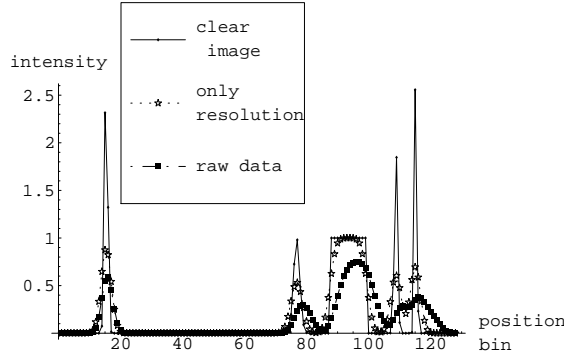


Figure 3: Test image and the response of the rectangular detector. In the first case we only apply the finite resolution of the detector, in the second case we apply first the parallax effect and second the finite resolution, giving us the simulated raw data.

figure 3. When we now apply our technique as given in formula 9, even making an error and assuming a better resolution of 2.9 bins instead of the simulated 3.7 bins, and using a relative cutoff of 5% (so we reject eigenvalues of the  $GP$  operator which are more than 20 times smaller than the largest eigenvalue), we can restore the image. Comparing it to the image we would have obtained with that detector if it had finite resolution, but no parallax effect, we obtain figure 4: the reconstruction is almost perfect.

In order to test the practical robustness of our technique, we introduce errors on some parameters for the parallax operator used during reconstruction. The sample distance is increased from 40cm to 43cm and the absorption coefficient is changed from 0.4 into 0.45 absorption lengths per cm. We also add random noise to the raw data (we added a uniformly distributed noise of relative intensity 2%). We apply the technique keeping the tolerance to 5%. We still obtain an image of reasonable quality, as shown in figure 5. Note that the small overall decrease in amplitude is normal due to the different absorption coefficients. The peaks at the right hand side are still well resolved, in the right position and of the correct relative amplitudes and widths, which is usually the information extracted in scattering experiments.

### 3.2 Case of a cylindrical detector.

We now consider a cylindrical geometry, with projection of the charges perpendicular onto a central wire. Although the geometry is more complicated in this case, and although now we have to consider not a ray (line) but a plane of radiation cutting through the entire cylinder, the idea behind the calculation of the parallax matrix elements is the same: a plane of radiation hitting (at the front

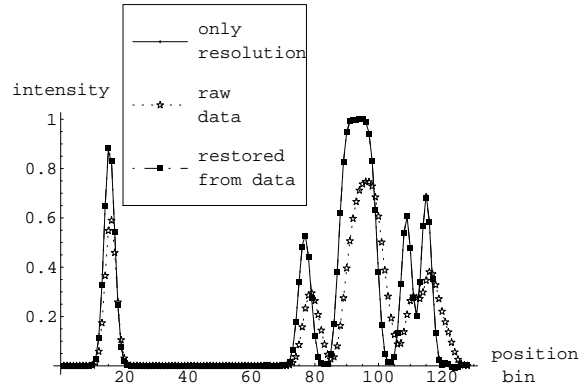


Figure 4: We compare the image the rectangular detector would have provided if it had finite resolution but no parallax effect, with the restored image using the raw data.

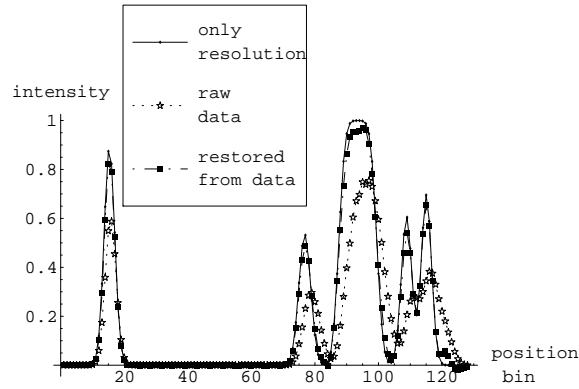


Figure 5: Reconstruction using slightly 'wrong' parallax and resolution parameters, and 2% relative noise added to the raw data.



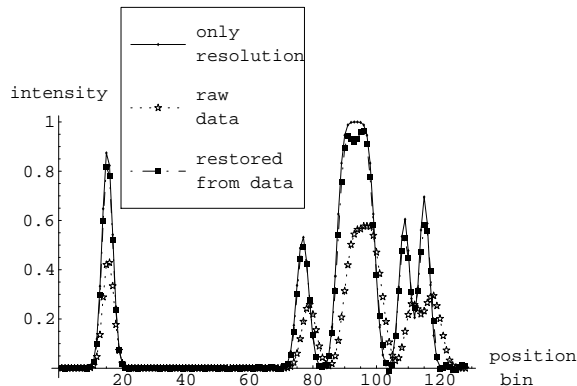


Figure 6: Cylindrical detector: the extracted picture from the raw data using our method is compared to what the detector would have done if there was only a finite resolution and no parallax effect. For the reconstruction, we've introduced geometrical errors, absorption length errors and we added noise to the raw data.

part of the cylinder) the middle of bin  $k$  will give rise to a certain probability of detection in the next few cells, and a geometrical calculation (together with an exponential absorption law) will allow us to obtain the parallax operator.

We've applied this to the following case: a tube of radius 1.2cm, of length 40cm, divided into 128 bins and a sample distance of 40cm. The absorption coefficient has been taken to be 0.4 absorption lengths per cm. We take the true resolution of the detector to be (FWHM) 3.7 bins.

Again introducing geometrical and detector parameter errors in the reconstruction to test practical robustness, we use an erroneous resolution of 2.9 bins instead of 3.7, together with a sample distance position of 42cm instead of 40cm, an absorption coefficient of 0.45 absorption lengths per cm instead of 0.4, and we add 2% of relative noise to the raw data. We use a cutoff of the singular values at 5% again. We then arrive at a restored image as shown in figure 6, which still gives a satisfying result, and the same comments apply as in the case of a rectangular detector volume.

## 4 Discussion.

After a theoretical explanation, we've tried to show, at the hand of realistic case studies, that even a severe parallax effect does not completely spoil the resolution of the image, and that useful information can be extracted, using the proposed inversion technique. Sometimes some tuning of the tolerance allowed in the truncated singular value decomposition is needed (especially in difficult

cases of strong parallax, badly known detector parameters and noisy data) in order to get most out of the data. We have to warn that we noticed that in the case of severe errors on the detector parameters, or very high levels of statistical noise, some small oscillations appear in the restored picture. So this technique works best when we know rather well the detector parameters and have data of relatively high statistical quality, even if the parallax effect is strong. Of course preventing parallax (using clever detector and instrument construction) is always better than to cure it, but we tried to show in this paper that a cure is possible for existing (or future) instruments and data suffering from parallax.

## References

- [1] S.Yu.Grachev and V.D. Peshekhonov, JINR Internal Report E13-96-83.
- [2] Yu.V. Zanevsky, S.P. Chernenko et *al.*, Nucl. Instr. Meth. A 367 (1995) 76-78
- [3] Yu.V. Zanevsky, S.P. Chernenko et *al.*, Nucl. Phys. B (Proc. Suppl.) 44 (1995) 406-408
- [4] V. Comparat et al, French patent n 2 630 829 (1988).
- [5] P. Rehak, G.C. Smith and B. Yu, IEEE Trans. Nucl. Sci., vol 44, no. 3 (1997) 651-655.
- [6] G. Charpak, Nucl. Instr. Meth. 201 (1982), 181-192.
- [7] R.A. Haddad and Th. W. Parsons, Digital Signal Processing, Theory, Applications and Hardware ©1991, W.H. Freeman and Company.
- [8] G.H. Golub and C. F. Van Loan, Matrix Computations, third edition, ©1996 John Hopkins University Press.